Hindawi
Advances in Materials Science and Engineering
Volume 2021, Article ID 6450251, 15 pages
https://doi.org/10.1155/2021/6450251

Research Article

Optimization of FSP Process Parameters on AA5052 Employing the S/N Ratio and ANOVA Method

C. Chanakyan,[1] S. Sivasankar,[1] M. Meignanamoorthy,[2] M. Ravichandran,[2] V. Mohanavel,[3] Saleh Alfarraj,[4] Hesham S. Almoallim,[5] Velu Manikandan,[6] and J. Isaac JoshuaRamesh Lalvani[7]

[1]*Department of Mechanical Engineering, Government College of Engineering, Thanjavur, Tamilnadu, India*
[2]*Department of Mechanical Engineering, K. Ramakrishnan College of Engineering, Tiruchirappalli 621112, Tamilnadu, India*
[3]*Centre for Materials Engineering and Regenerative Medicine, Bharath Institute of Higher Education and Research, Selaiyur, Chennai 600073, Tamil Nadu, India*
[4]*Zoology Department, College of Science, King Saud University, Riyadh 11451, Saudi Arabia*
[5]*Department of Oral and Maxillofacial Surgery, College of Dentistry, King Saud University, PO Box-60169, Riyadh 11545, Saudi Arabia*
[6]*College of Environmental & Bioresource Sciences, Chonbuk National University, Iksan 570752, Republic of Korea*
[7]*Department of Mechanical Engineering, Faculty of Mechanical and Production Engineering, AMIT, Arbaminch University, Arba Minch, Ethiopia*

Correspondence should be addressed to J. Isaac JoshuaRamesh Lalvani; isaac.jrl@amu.edu.et

Received 3 August 2021; Accepted 7 September 2021; Published 11 October 2021

Academic Editor: P Ganeshan

AA5052 bead-on-plate processing has been achieved by the friction stir processing (FSP) technique to examine the manipulation of process parameters. It also improved the base metal surfaces to analyze the microstructure. The tool spinning speed, traverse speed, and axial load were preferred to investigate the effect of friction stir bead-on-plate processing on the tensile strength qualities and microhardness in AA5052. An optical microscope was used to dissect the fabricated processed zones of the microstructure. By using the design of the experiment, the orthogonal array of the L9 Taguchi method was used to construct the processing experiments. The analysis of variance and the signal-to-noise ratio methods were employed to identify the optimum unification of process parameters and the significant benefaction of a specific parameter on the responses. The outcomes showed that the tool spinning speed was the principal factor affecting the characteristics of tensile strength and microhardness, succeeded by the traverse speed and axial load. The intermetallic compound layer had formed during the processing under specified conditions. This examination revealed that the optimum parameters could intensify the mechanical behaviour of AA5052.

1. Introduction

Various materials of welding with appropriate mechanical finishing and high surface completion are essential for the processing of bead-on-plate welding. The properties of joints depend basically on the processing systems, base metal material properties, types of processed joints, the region of heat-influenced and metallurgical changes during bead-on-plate processing, and process parameters. The joining process is a secure-state method. It has different favourable circumstances over the standard fusion welding process, for example, excellent mechanical properties and comfort, no utilization of consumable material, and work in all positions. There have been numerous exploration projects with a broad scope, allowing for the benefits provided by FSP. Strengths of FSP and the impact of process parameters, namely, tool rotation speed, traverse speed, and axial load, are generally researched. Because of the motivation given by its application in the aviation, marine work, railroad, and transport industries, the FSP procedure is utilized in practically all mechanical segments. Investigational outcomes were measurably handled by analysis of variance (ANOVA) in the

Taguchi technique to forecast the optimized process parameters for friction stir processing (FSP). The results demonstrate that the rotational tool speed, traverse speed, and axial load process parameters have altogether influenced the tensile strength properties and microstructure of the bead-on-plate processed joints.

Cavaliere et al. examined the effect of FSW process parameters on tensile properties and the microstructure of joints of AA6056. Joints were created at the rotational speeds of 550, 850, and 1,050 rpm and traverse speeds of 44, 58, and 70 mm/min. According to the findings, the strongest material strengthening occurs at a traverse speed of 58 mm/min, and it decelerates at a rotating tool speed of 550 rpm. Additionally, it raises the rotational speed of the tool and welding speed and diminishes strength [1]. Minton et al. processed the aluminium composites of 6082-T6 with 6.5 and 4.5 mm thicknesses of welds with the assistance of a FSW milling machine with suitable clamping devices. The results revealed that the vertical milling machine has been equipped for processing the material. Microhardness of the processed joints changes in the range of 52 and 82% of the base material microhardness [2]. Elangovan et al. studied the traverse speed effect and FSW for AA2219 combination influenced by the tool pin profile. A different form of tool pin profiles (TPPs) like straight cylindrical-shaped, conical cylinder, threaded cylinder, triangular, and square is used to manufacture welding processing at various welding speeds of 0.36, 0.66, and 1.35 mm/sec. The results showed that the square tool pin profile had been formed mechanically and flaw-free welds contrasted with different tool pin profiles [3]. Jayaraman et al. studied the optimized parameters (axial load, welding, and rotational tool speed) of the FSW process for rigidity of aluminium 319 composites with the Taguchi technique. To combine the estimated tensile strength and process parameters, they created a numerical model by grey relational analysis. The ultimate tensile strength was found at 1200 rpm of rotational tool speed, 45 mm/min of traverse speed, and 4 kN of axial load [4]. Aydin et al. investigated the impact of elongation and tensile strength utilizing the Taguchi technique, and it was established by the grey relational analysis. Traverse speed, rotational speed, and tool shoulder diameter were used to analyze the FSW process in AA1050. They verified the possibility of using the Taguchi technique with the grey relational method for improving welding quality. The weight estimations were finished by using the analytical hierarchy process (AHP), and the loads were observed to be 0.30 and 0.70 N for tensile strength and elongation responses, respectively [5]. Lian et al. recommended a numerical technique empowered with grey relational analysis to construct a systematic method for investigating the concept of design evaluation. The results revealed that the proposed coarse grey relational investigation has a different option for evaluating the concept of design. The unclear primary information and design were displayed and investigated adequately and analytically [6]. Chi-hui et al. enhanced friction stir processing on AA5083 composites by utilizing the GRA technique with the Taguchi design. The process parameters were pin profile length, rotational speed, tilt angle, and traverse speed. The natural factors are the extreme tensile strength and elongation for the processed material. An outcome with 1800 rpm rotational speed and 180 mm/min welding speed at 180 mm/min, 10° tilt angle of the tool, and 2.5 mm pin length was optimum for finishing quality with minimum expense [7]. Mithra et al. used the Taguchi strategy with the grey relational method to decide various characteristics of drilling quality in the laser process. They showed the possibility of using the grey-Taguchi method for constant enhancement of the quality of fabricated products. The final results showed that the development of a tapered hole is 16.30 and 8.78 percent from the start to the optimal location [8]. Karun Kumar et al. analyzed the solid-state welding process using AA5052. Pentagonal and square pin profiles were used for welding the two pieces of the base plate. Aluminium alloy (AA) 5052 is broadly used in sheet metal work, gas-in-fuel tankers, ships, and aircraft. The parameters, such as axial load, welding speed, tool pin profiles, and tool rotation speed, play a significant role in friction stir processing of AA5052. During this investigation, the use of pentagonal pin profiles in the friction stir welding obtained excellent welds compared to the square pin profile. Three various traverse speeds of 40, 60, and 80 mm/min were considered. The enhancement in mechanical properties was identified while using the pentagon pin profile at 60 mm/min traverse speed [9]. Shanavas et al. addressed the prediction of weld quality in AA5052 with significant parameters of friction stir welding. They developed a regression and a fuzzy logic model for improving the quality of tensile strength and % elongation. The central composite design was used to perform the welding in AA5052 to obtain the maximum tensile stability of welded joints and its outcomes compared with the statistical method. The developed model demonstrated the confidence level at 95% efficiently. The fuzzy model was predicted and used to obtain an acceptable output with minor errors compared to the statistical method [10]. Venkateshkannan et al. compared the distinctive tool pin profiles such as cylindrical threaded, squared, cylindrical, step, and tapered. Dissimilar friction stir welding was executed on AA2024 and AA5052. The SEM and microstructure analysis obtained the mechanical characteristics. Among the different pin profiles, tapered and cylindrical pins exhibited the minor level of discontinuities in macrograph outputs. They determined the optimal parameters of 1000 rpm of tool spinning speed and 40 mm/min of feed. Using step pin profiles achieved the highest tensile strength (297 MPa) on dissimilarly welded base plates [11].

Friction stir processing is a method for processing different alloy components. In this investigation, the bead-on-plate processing method is a preprocessing technique to develop the properties of base metal surface [12]. A spinning tool is infused into the base metal plate surfaces and passed through the length of the plate for processing. Frictional heat produced by the tool spinning against the workpiece makes it delicate and plastically deformed. Rotational and traverse developments of the tool pin strengthen the processing of the base material. The Taguchi method recognizes the optimum level of process parameters for the mechanical characteristics of the bead-on-plate specimen. Besides, the ANOVA found the percentage contribution of the processed

parameters. An optical microscope was able to investigate the microstructure as fine as the processed surfaces of the fabricated bead-on-plate processing.

2. Experimental Procedure

2.1. Materials and Processing. For this experiment, aluminium alloy (AA) 5052 was selected for friction stir bead-on-plate processing. The excellent formability and good weldability were of concern in the base material. AA5052 is composed of basically a superplastic material and is easily made from ultra-refinement structures during the friction stir processing. In the present day, the base material is used in aircraft, marine, and vehicle industries for structural applications. The mechanical properties of AA5052 are 251.34 MPa tensile strength, 19% elongation, and 70 Hv microhardness, and its chemical composition is presented in Table 1. In this study, FIE (from India) (tensile strength testing machine) with the standard of ASTM E9 and Shimadzu HMV-G (microhardness tester) with the standard of ASTM B724 were utilized to conduct the mechanical test. In this investigation, the normal hardness test does not attain the strength of the processed specimens due to low weight being added during the test. But, the FSPed specimen surface was covered by the onion ring structure. It is revealed that microhardness was a key factor to measure the strength with the maximum load capacity of the processed specimen. The base materials prepared have the dimensions of 100 mm × 100 mm × 6 mm. In this study, high carbon high chromium die steel (HCHCr) was utilized as a tool material for the bead-on-plate friction stir processing due to its high toughness and wear-resistant property. Normally, HCHCr is ceramic-based tool material, and it possesses microhardness 10 times higher than of the base material to enhance the material properties. The pentagonal tool pin profile was obtained by surface grinding and CNC. The dimension of the pentagonal tool pin profile was 5.7 mm pin length and 18 mm shoulder diameter [13]. Figures 1(a) and 1(b) show the tool pin profile and friction stir processing. The required size of the base metal marked with a centre line, and the influence of the pentagonal pin profile produced the onion ring structure on the surface of the material to manipulate the characteristics [14]. Figures 2(a) and 2(b) show the friction stir processed image and the prepared tensile specimens, respectively.

2.2. Method of Process Parameters. The optimization of friction stir bead-on-plate process parameters was designed by the Taguchi technique and used to form the orthogonal arrays, which consider a smaller amount of experimentation among a large number of decision variables. Signal-to-noise proportions were used to measure and predict the quality of the responses. Lowest and moderate improvement costs can be achieved by this efficient process. Transformation of the experimental data into the required decision was performed by the analysis of variance (ANOVA). The Taguchi technique was used to prefer the most reasonable orthogonal array to design the experiments and to consign process parameters [15]. Various researchers found the optimal specimens below the specified parameters within the limit. Based on the literature review, the parameters of friction stir bead-on-plate processing were preferred, and the level of each bead-on-plate process parameters for the three factors is presented in Tables 2 and 3, individually. During the hardness test, each plate has 20 values that are marked in the mid-section of the processed plates. In the current study, the percentage contribution of processed parameters to the mechanical properties was determined and successfully implemented by ANOVA. By using the statistical software of MINITAB, the investigational responses were modified into the S/N ratio. Table 4 describes the estimated S/N ratio values.

3. Results and Discussion

3.1. Influence of Process Parameters on the Tensile Strength. Table 5 presents the response table for tensile strength and S/N ratio. From the response table, tool spinning speed is the most significant influencing factor on the tensile strength, accompanied by traverse speed and axial load. Accordingly, an increase in tool spinning speed to advance the maximum friction occurs between the tool and the base material 5052 aluminium alloy, thus delivering high temperatures at the interface of the processed specimen, which helps in increasing the tensile strength. Similarly, increasing the traverse speed increases the tensile strength. Figures 3(a)–3(c) exhibit the graph of mean of S/N ratios for tensile strength versus process parameters such as tool spinning speed, traverse speed, and axial load. It is exposed that the maximum tensile strength attained by the optimum level of process parameter unifications is $A_2B_3C_2$, which shows the tool spinning speed at level 2 (1000 rpm), traverse speed at level 3 (30 mm/min), and axial load at level 2 (5 kN). Table 6 displays the ANOVA outcomes for tensile strength. It is validated that the tool spinning speed is the most significant process parameter with a 91.8% contribution, succeeded by an axial load of 5.04%. The traverse speed is a less significant process parameter with a 3.09% contribution. The 99.79% *R*-Sq value of tensile strength conceded that the model is capable of predicting the response with greater efficiency [16].

The interaction influence of process parameters, such as tool spinning speed, traverse speed, and axial load, on the tensile strength is displayed in Figures 4(a)–4(c). From the interaction graph, the parallel line and nonparallel line show no interaction and significant interaction of the process parameters on the tensile strength, respectively. In Figure 4(a), the interactions of the tool spinning speed with traverse speed were significant at the tool spinning speed of 1000 rpm. Therefore, it is clearly explained that the increase in the tool spinning speed increases the tensile strength. Figure 4(b) shows the interactions between the tool spinning speed and axial load. It is revealed that increasing the tool spinning speed led to increase in the tensile strength at 1000 rpm. The interaction of traverse speed with tool spinning speed is significant at 1000 rpm tool spinning speed and 20 mm/min traverse speed, due to the reason that lower

Table 1: Chemical composition of the AA5052 base plate.

Components	Mg	Fe	Cr	Mn	Si	Cu	Zn	Al
Weight in %	2.5	0.3	0.2	0.1	0.1	0.1	0.1	Bal

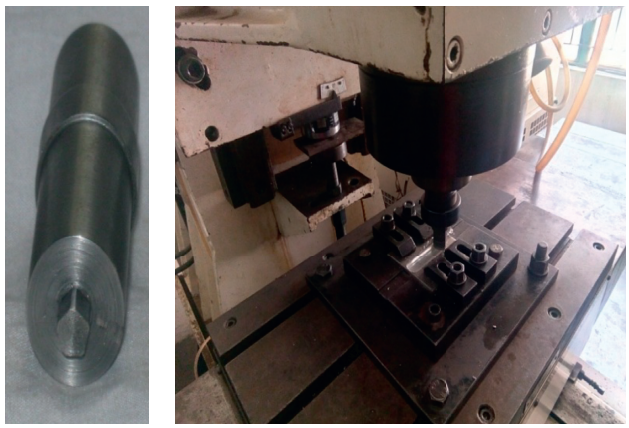

(a) (b)

Figure 1: (a) Pentagonal tool pin profile and (b) friction stir processing.

(a) (b)

Figure 2: (a) Friction stir processed image and (b) prepared tensile specimens.

traverse speed increases the tensile strength for the entire tool spinning speed as shown in Figure 4(c). Consequently, the tensile strength of the AA5052 processed specimen decreased for the high axial load (7 kN) if tool spinning speed (1200 rpm) and traverse speed (20 mm/min) were high, although moderate tool spinning speed (1000 rpm), low traverse speed (20 mm/min), and the medium level of axial load (5 kN) produced higher tensile strength [17].

The contour plots for the tensile strength for inconstant process parameters are demonstrated in Figures 5(a)–5(c). Figure 5(a) exhibits the influence of the tool spinning speed and axial load on the tensile strength. It is revealed that the tensile strength increases with the increase in tool spinning speed at any axial load. Still, at the lower tool spinning speed, the axial load caused the increase in the tensile strength to be less in the processed specimen. It is explained that the maximum tensile strength (215 MPa) was obtained at the medium level of axial load and the moderate level of tool spinning speed. The influence of traverse speed and axial load on the tensile strength is demonstrated in Figure 5(b). It is perceived that the moderate level of axial load and lower level of traverse speed achieved better tensile strength (209 MPa) due to sufficient heat produced in the nugget region. The higher level of axial load and traverse speed achieved the poor tensile strength due to insufficient heat between the tool and specimen. Figure 5(c) displays the influence of the tool spinning speed and traverse speed on the tensile strength. It is revealed that the maximum tensile strength was achieved at the moderate level of tool spinning speed (1000 rpm) and a lower level of traverse speed (20 mm/min).

Table 2: FSP parameters and factor levels.

Bead-on-plate process parameters	Notation	Factor levels		
		1	2	3
Tool spinning speed (rpm)	TSS (A)	800	1000	1200
Traverse speed (mm/min)	TS (B)	20	25	30
Axial load (kN)	Al (C)	3	5	7

Table 3: Design of the experimentation by using the L9 orthogonal array.

Runs	TSS (rpm)	TS (mm/min)	AL (kN)
1	800	20	3
2	800	25	5
3	800	30	7
4	1000	20	5
5	1000	25	7
6	1000	30	3
7	1200	20	7
8	1200	25	3
9	1200	30	5

3.2. Influence of Process Parameters on the Microhardness. Table 7 presents the response table for microhardness means and S/N ratio. From the response table, tool spinning speed is the most significant influencing factor on the microhardness, accompanied by traverse speed and axial load. Accordingly, an increase in tool spinning speed to advance the maximum friction occurs between the tool and the base material 5052 aluminium alloy, thus delivering high temperatures at the interface of the processed specimen, which helps in increasing the microhardness. Similarly, increasing the traverse speed led to increase in the microhardness. Figures 6(a)–6(c) exhibit the graph of mean of S/N ratios for microhardness with respect to process parameters such as tool spinning speed, traverse speed, and axial load. It is exposed that the maximum microhardness attained by the optimum level of process parameter unifications is $A_2B_3C_2$, which shows the tool spinning speed at level 2 (1000 rpm), traverse speed at level 3 (30 mm/min), and axial load at level 2 (5 kN). Table 8 displays the ANOVA outcomes for microhardness. It is validated that the tool spinning speed is the most significant process parameter with a 60.8% contribution, succeeded by an axial load of 29.66%. The traverse speed is a less significant process parameter with a 9.48% contribution. The 99.70% *R*-Sq value of tensile strength conceded that the model is capable of predicting the response with greater efficiency [18].

The interaction influence of process parameters, such as tool spinning speed, traverse speed, and axial load, on the microhardness is exhibited in Figures 7(a)–7(c). From the interaction graph, the parallel line and nonparallel line show no interaction and significant interaction of the process parameters on the tensile strength, respectively. Figure 7(a) shows that the interactions of tool spinning speed with traverse speed were significant at the tool spinning speed of 1000 rpm. Therefore, it is clearly explained that the increase in the tool spinning speed increases the microhardness value. Figure 7(b) shows the interactions between the tool spinning speed and axial load. It is revealed that increasing the tool spinning speed led to the increase in microhardness at 1000 rpm. The interaction of traverse speed with tool spinning speed is significant at a tool spinning speed of 1000 rpm and traverse speed of 20 mm/min, due to the reason that lower traverse speed increases the microhardness for the tool spinning speed as shown in in Figure 7(c). Therefore, the microhardness of the AA5052 processed specimen decreased for the high axial load (7 kN) if tool spinning speed (1200 rpm) and traverse speed (20 mm/min) were high, although moderate tool spinning speed of 1000 rpm, low traverse speed of 20 mm/min, and the medium level of axial load of 5 kN produced higher microhardness.

The contour plots for the microhardness for variable process parameters are established in Figures 8(a)–8(c). Figure 8(a) displays the influence of the tool spinning speed and axial load on the microhardness. It is exposed that the microhardness value increases with increase in tool spinning speed at an axial load of 5 kN. However, at the lower tool spinning speed, the axial load caused the decrease in the microhardness in the processed specimen. It is explained that the maximum microhardness (69 Hv) was obtained at the medium level of axial load and the moderate level of tool spinning speed. The influence of traverse speed and axial load on the microhardness is demonstrated in Figure 8(b). It is perceived that the moderate level of axial load and lower level of traverse speed achieved better microhardness (68 Hv). The higher level of axial load and traverse speed achieved less microhardness value due to insufficient heat produced between the tool and specimen. Figure 8(c) displays the influence of the tool spinning speed and traverse speed on the microhardness. It is revealed that the maximum microhardness was achieved at the moderate tool spinning speed (1000 rpm) and a lower traverse speed (20 mm/min).

3.3. Regression Equation of Tensile Strength and Microhardness. The regression equation is refined based on the investigational output responses. It establishes the

Table 4: Estimated S/N ratio values.

Runs	Parameters			Response of the output		S/N ratio of the output	
	TSS (rpm)	TS (mm/min)	AL (kN)	Tensile strength (MPa)	Microhardness	Tensile strength (MPa)	Microhardness
1	800	20	3	173	61	44.7609	35.70
2	800	25	5	184	66	45.2964	36.40
3	800	30	7	183	64	45.2490	36.12
4	1000	20	5	215	69	46.6488	36.78
5	1000	25	7	213	68	46.5676	36.65
6	1000	30	3	212	67	46.5267	36.52
7	1200	20	7	169	61	44.5577	36.71
8	1200	25	3	170	62	44.6090	35.85
9	1200	30	5	185	66	45.3434	36.39

Table 5: Response table for tensile strength.

Level	TSS (A)	TS (B)	AL (C)
S/N ratio of tensile strength			
1	45.10	45.32	45.30
2	46.58	45.49	45.76
3	44.84	45.71	45.46
Delta	1.74	0.38	0.46
Rank	1	3	2
Mean of tensile strength			
1	180.0	185.7	185.0
2	213.3	189.0	194.7
3	174.7	193.3	188.3
Delta	38.7	7.7	9.7
Rank	1	3	2

equivalence between the input process parameters for friction stir processing. Regression equations (1) and (2) provide the equivalence between the measured process parameters to produce the maximum tensile strength and microhardness [19]. Figures 9(a) and 9(b) exhibit the comparison plots for investigational and regression-predicted values of tensile strength and microhardness:

$$\text{tensile strength (MPa)} = 179.3 - 0.0133\,\text{tool spinning speed (rpm)} + 0.77\,\text{traverse speed (mm/min)} + 0.83\,\text{axial load } (k\text{N}), \tag{1}$$

$$\text{microhardness (Hv)} = 60.3 - 0.0167\,\text{tool spinning speed (rpm)} + 0.200\,\text{traverse speed (mm/min)} + 0.250\,\text{axial load (kN)}. \tag{2}$$

3.4. Microstructure Analysis. In the friction stir bead-on-plate processing of AA5052, a diversity of microstructure is captured in different zones using an optical microscope (Dewinter Inverted Trinocular). The microstructure outcomes showed the structure of grain refinement in the various zones (nugget zone, thermomechanically affected zone, and heat-affected zone) of the processed aluminium alloy 5052. The shape and size of the nugget zone for optimal processed samples were realized depending on the bead-on-plate process parameters and the interaction of the base material with the pentagonal pin profile tool and its shoulder. The microscopic picture showed reflection of the optimal value of the input factors with output response of tensile strength [20]. The microstructure image was captured within the limitation of 100x and 100 μm. Figure 10(a) shows the AA5052 base metal of the microstructure. Figures 10(b)–10(d) exhibit the cross section of the bead-on-plate processing, processed at 1000 rpm, 20 mm/min, and 5 kN, besides with different zones identified. The thermomechanically affected zone surrounded the nugget regions. The NZ (nugget zone) changes in the fine-grained morphological structure. The main inference behind the microstructure reformation is due to the accomplished thermal cycle during the processing phase. The interface of the nugget zone was characterized by the direction of tool spinning speed and traverse speed. The heat-affected zone (HAZ) enveloped the thermomechanically affected zone (TMAZ). In HAZ, the grain formation does not refine any plastic deformation. The microstructural region was slightly modified in the heat-affected zone [21]. Figures 11(a)–11(c) and Figures 12(a)–12(c) expose the blemish-free processed samples obtained by friction stir bead-on-plate processing at 1200 rpm,

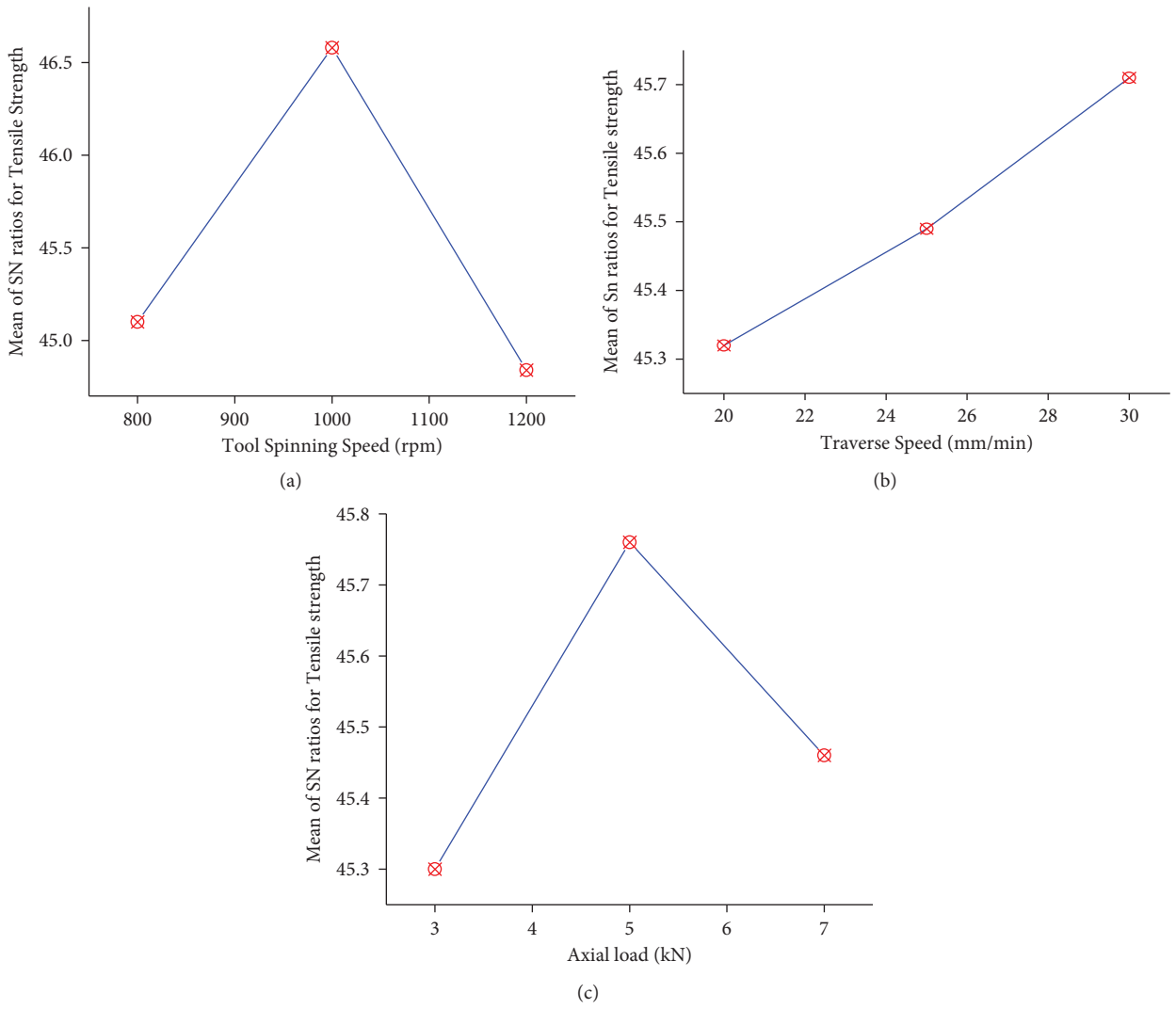

Figure 3: Mean of S/N ratios for (a) tensile strength versus tool spinning speed, (b) tensile strength versus traverse speed, and (c) tensile strength versus axial load.

Table 6: ANOVA outcomes for tensile strength.

Process parameters	DF	% contribution	Adj SS	Adj MS	F ratio	*P* value
TSS	2	91.8	2634.67	1317.33	439.11	0.002
TS	2	3.09	88.67	44.33	14.78	0.063
AL	2	5.04	144.67	72.33	24.11	0.040
Residual error	2	0.07	6.00	3.00		
Total	8	100	2874.00			

$S = 1.7321$; R-Sq = 99.79%; R-Sq (adj) = 99.61.

30 mm/min, and 5 kN and 1200 rpm, 20 mm/min, and 7 kN—the sound of defect-free processed AA 5052 specimens. The natural bond interface and the interblended structure were composed between the top and bottom of the processed specimens. The characteristic microstructural regions, such as the nugget zone, thermomechanically affected zone, heat-affected zone, and the base metal, were examined. Due to the effect of the thermal cycle and plastic deformation generated by the tool spinning speed, the dynamic recrystallization transpired in the nugget zone. The various the locations of the nugget zone, the different the forms of fine equiaxed grains formed. The coarse grain structure occurred in the different locations of TMAZ as shown in Figures 11(b) and 12(b), respectively [22].

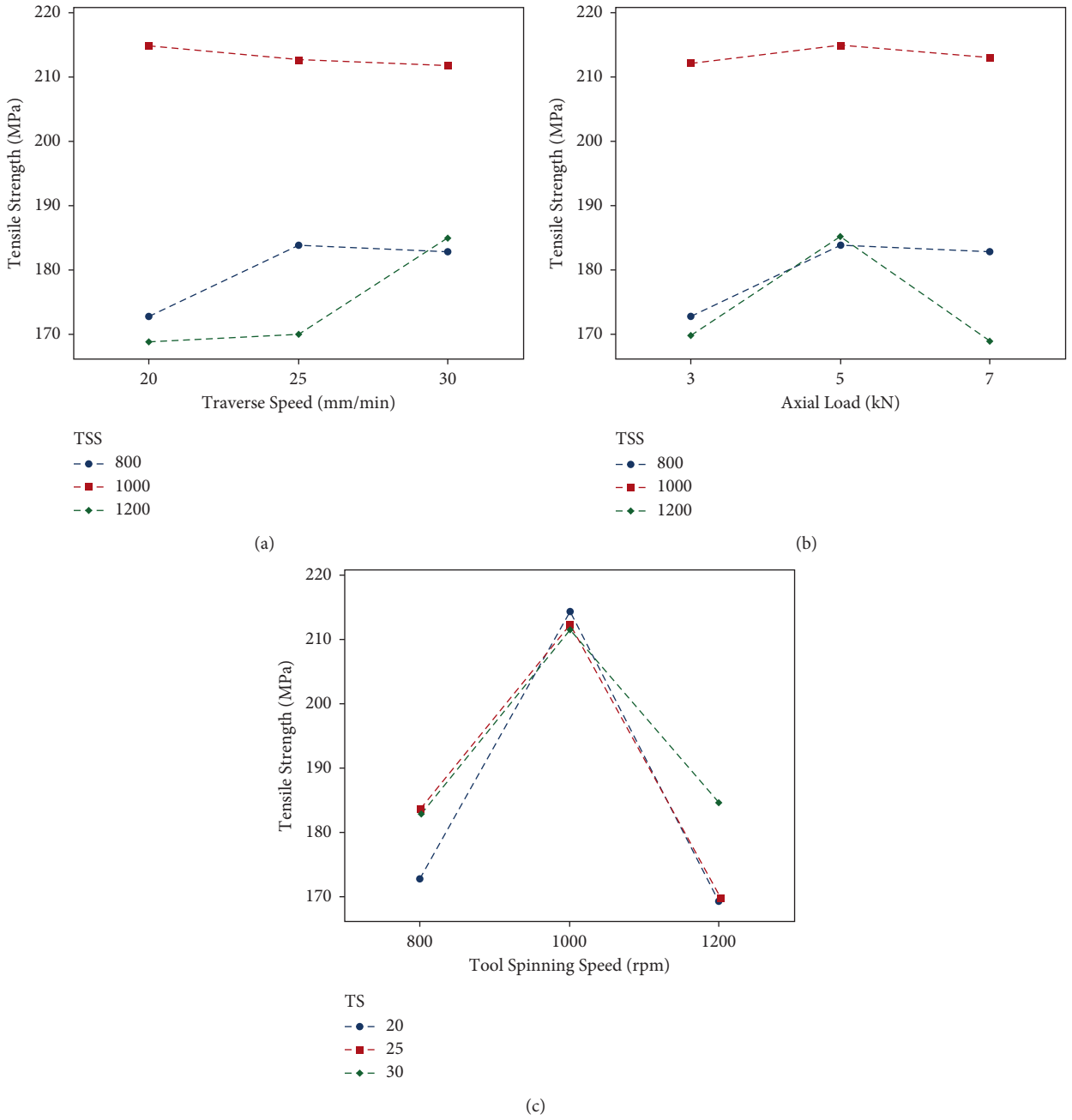

Figure 4: Interaction plots of tensile strength for (a) tool spinning speed versus traverse speed, (b) tool spinning speed versus axial load, and (c) traverse speed versus tool spinning speed.

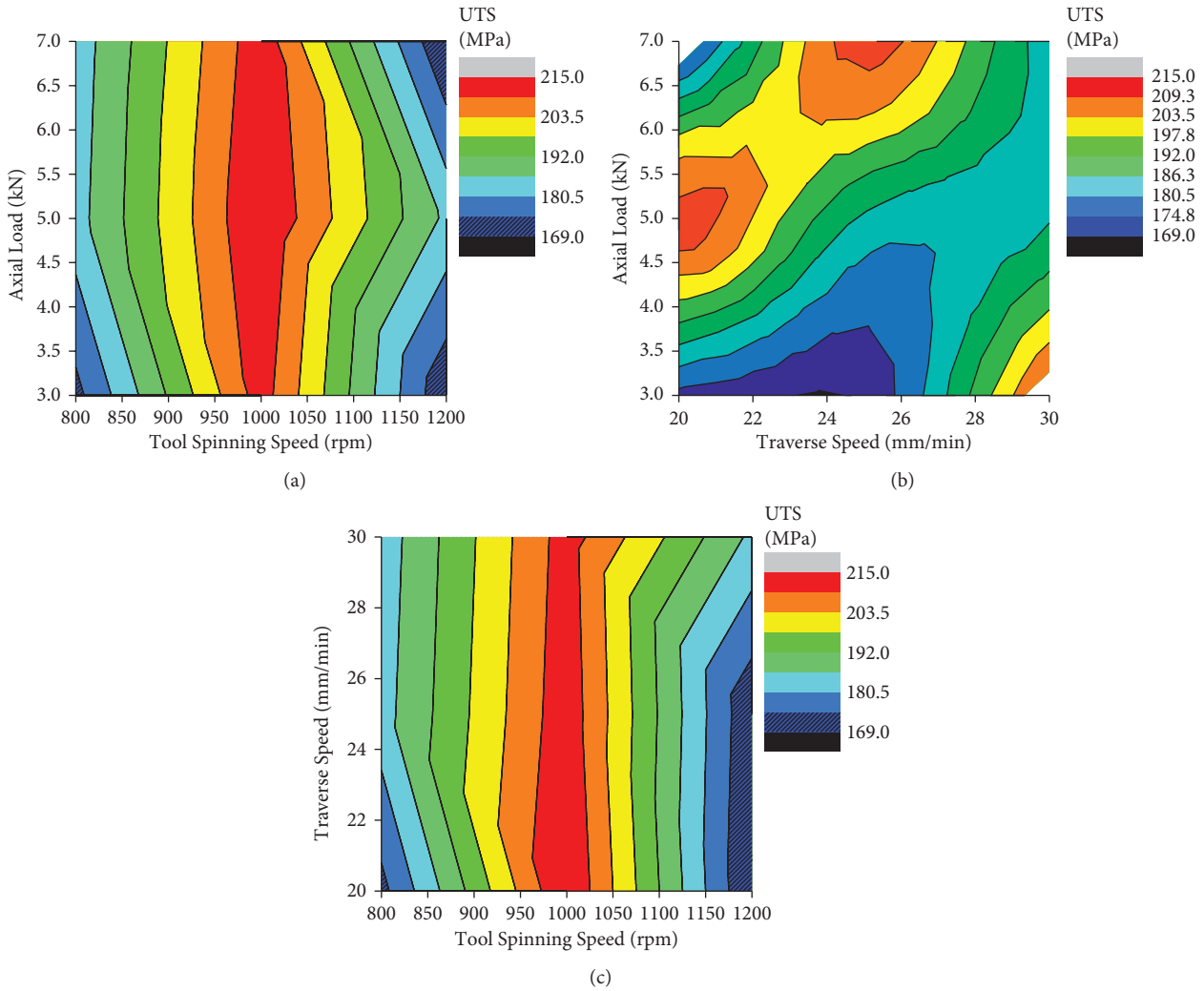

Figure 5: Contour plot of tensile strength for (a) tool spinning speed versus axial load, (b) traverse speed versus axial load, and (c) tool spinning speed versus traverse speed.

Table 7: Response table for microhardness.

Level	TSS (A)	TS (B)	AL (C)
S/N ratio of microhardness			
1	36.07	36.06	36.03
2	36.65	36.03	36.52
3	35.98	36.35	36.16
Delta	0.67	0.28	0.49
Rank	1	3	2
Mean of microhardness			
1	63.67	63.67	63.33
2	68.00	65.33	67.00
3	63.00	65.67	64.33
Delta	5.00	2.00	3.67
Rank	1	3	2

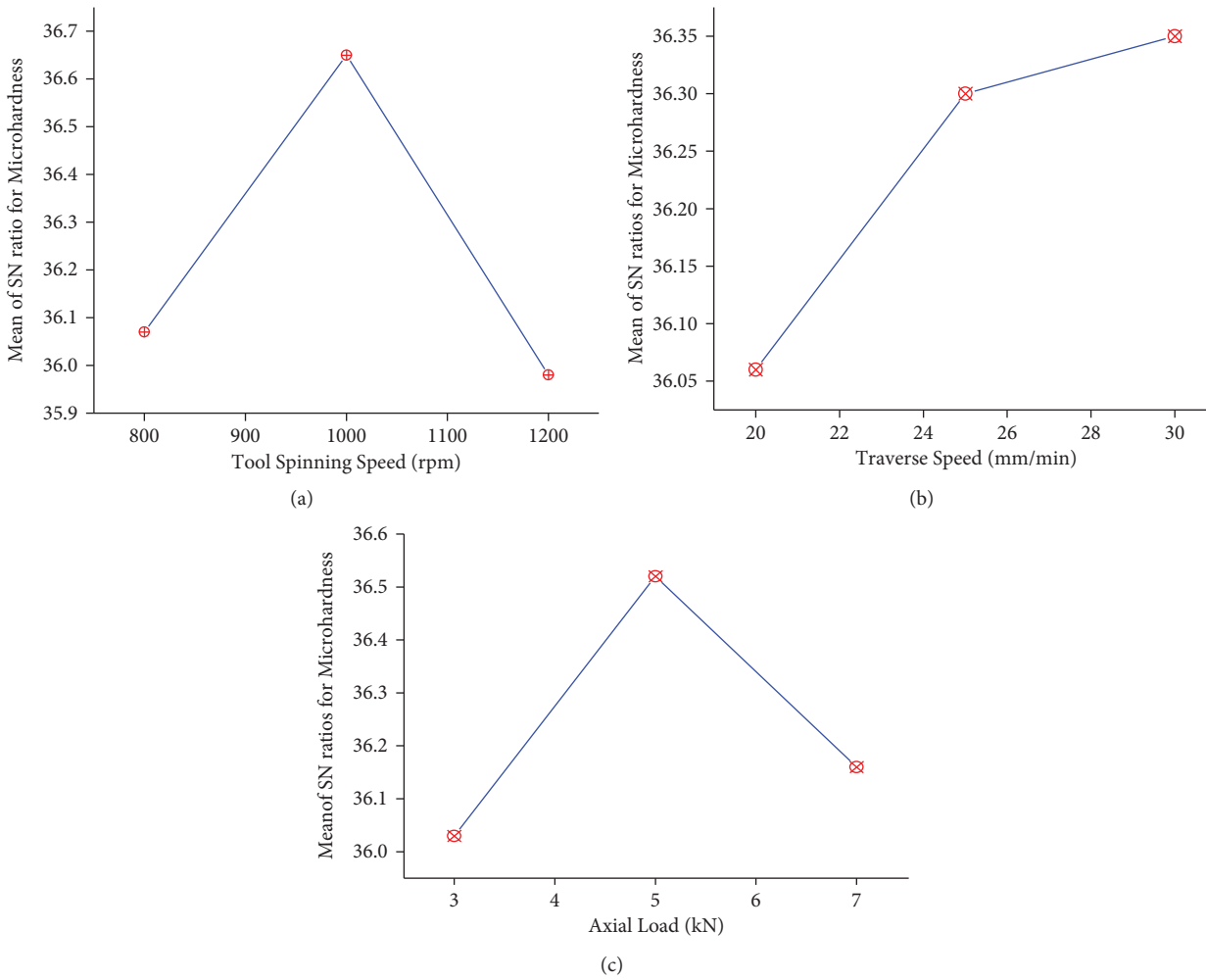

Figure 6: Mean of S/N ratios for (a) microhardness versus tool spinning speed, (b) microhardness versus traverse speed, and (c) microhardness versus axial load.

Table 8: ANOVA outcomes for microhardness.

Process parameters	DF	% contribution	Adj SS	Adj MS	*F* ratio	*P* value
TSS	2	60.8	44.2222	22.1111	199.00	0.005
TS	2	9.48	6.8889	3.4444	31.00	0.031
AL	2	29.66	21.5556	10.7778	97.00	0.010
Residual error	2	0.06	0.2222	0.1111		
Total	8					

$S = 0.3333$; R-Sq = 99.70%; R-Sq (adj) = 98.78.

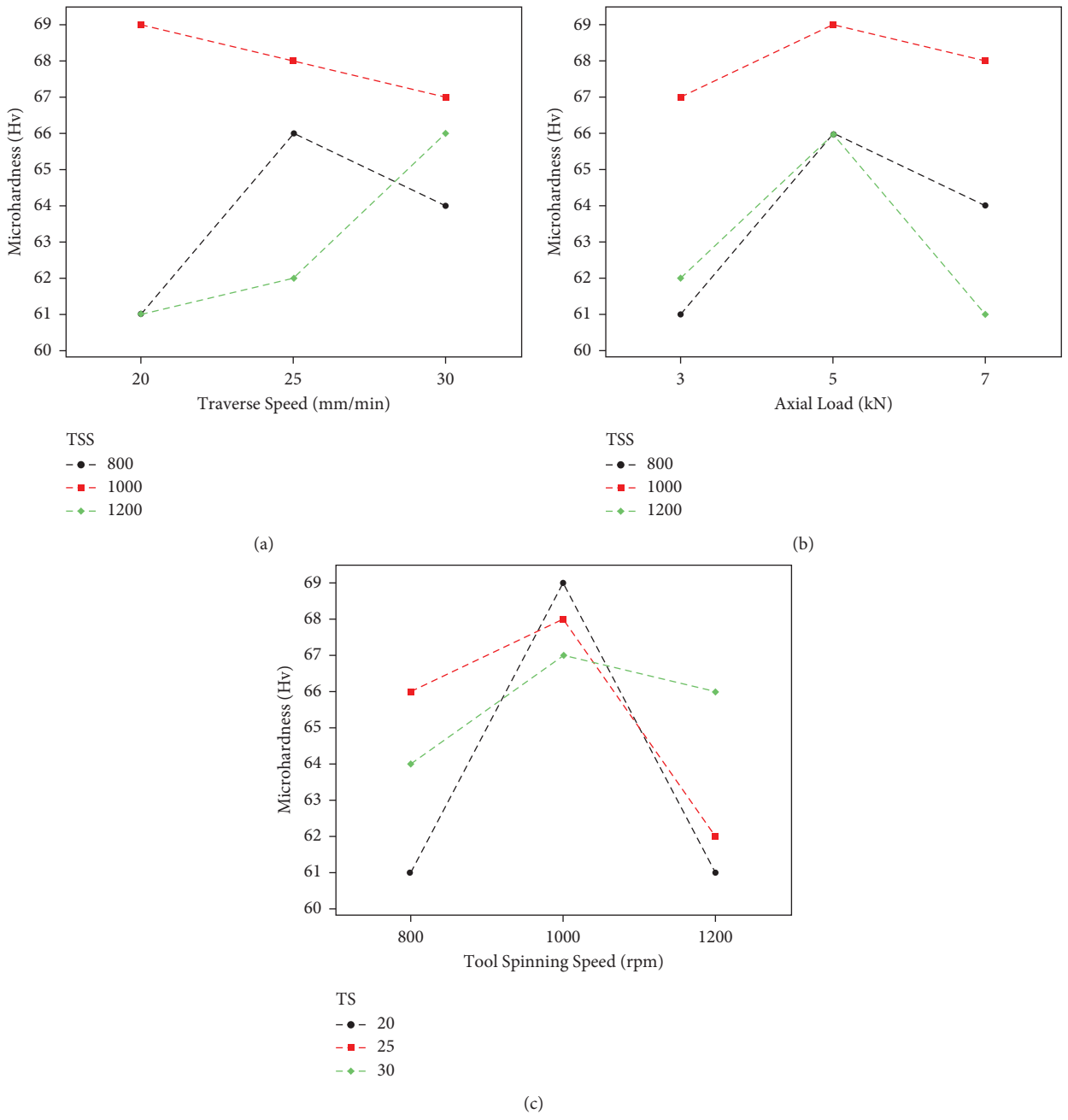

FIGURE 7: Interaction plots of microhardness for (a) tool spinning speed versus traverse speed, (b) tool spinning speed versus axial load, and (c) traverse speed versus tool spinning speed.

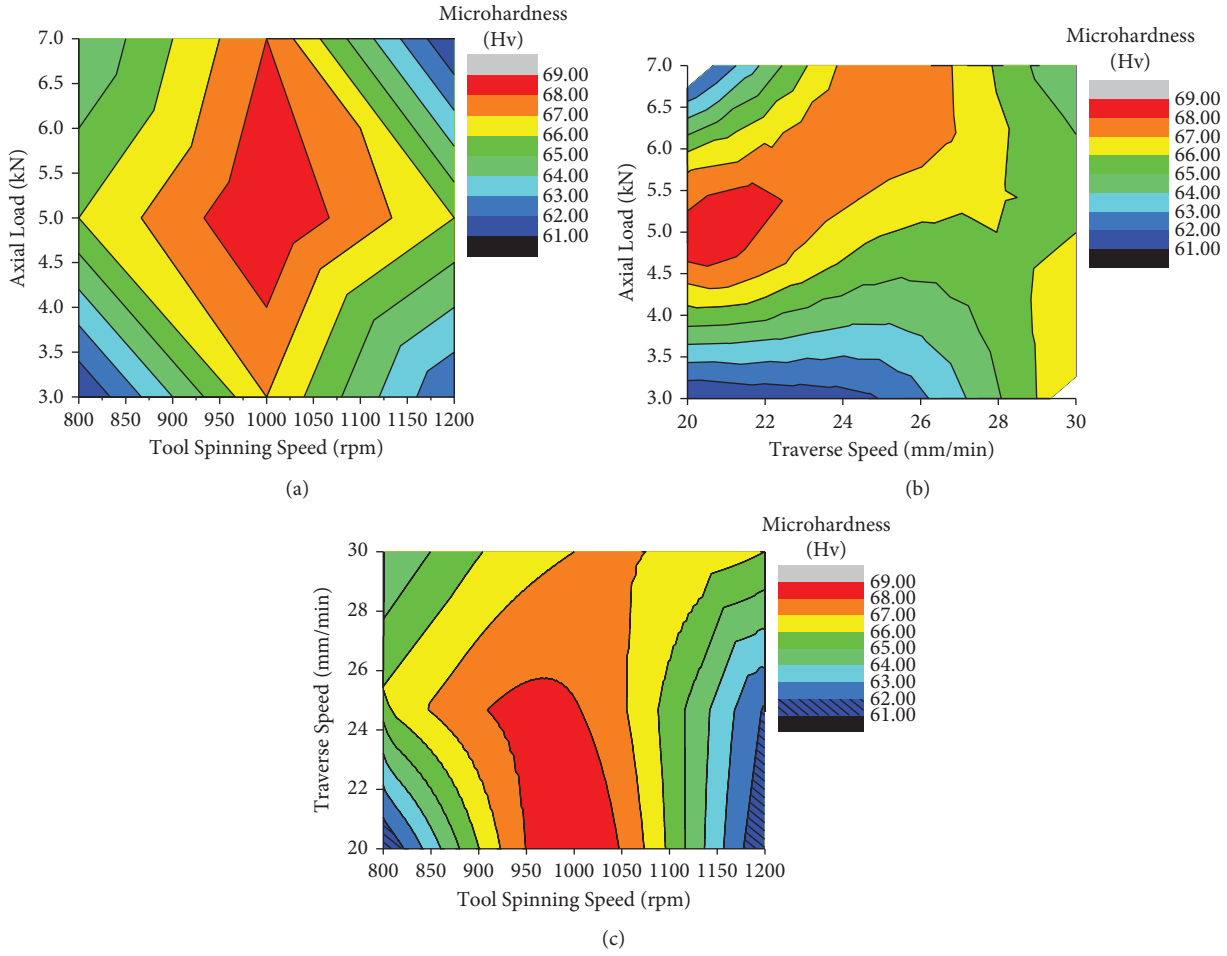

Figure 8: Contour plots of microhardness for (a) tool spinning speed versus axial load, (b) traverse speed versus axial load, and (c) tool spinning speed versus traverse speed.

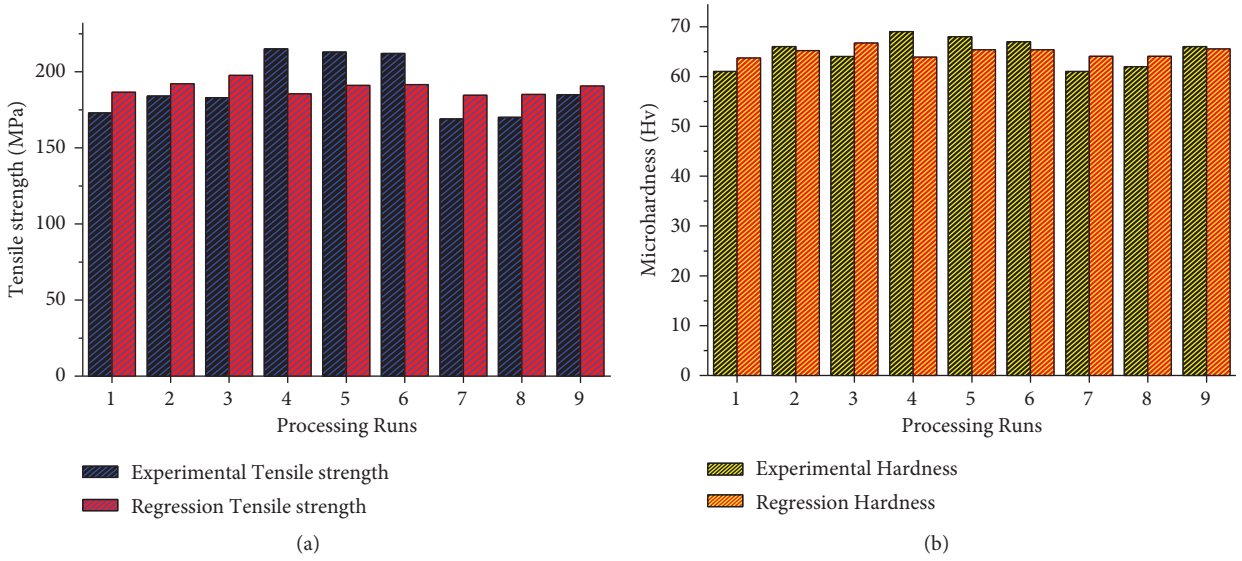

Figure 9: Experimental and regression values of (a) tensile strength and (b) microhardness.

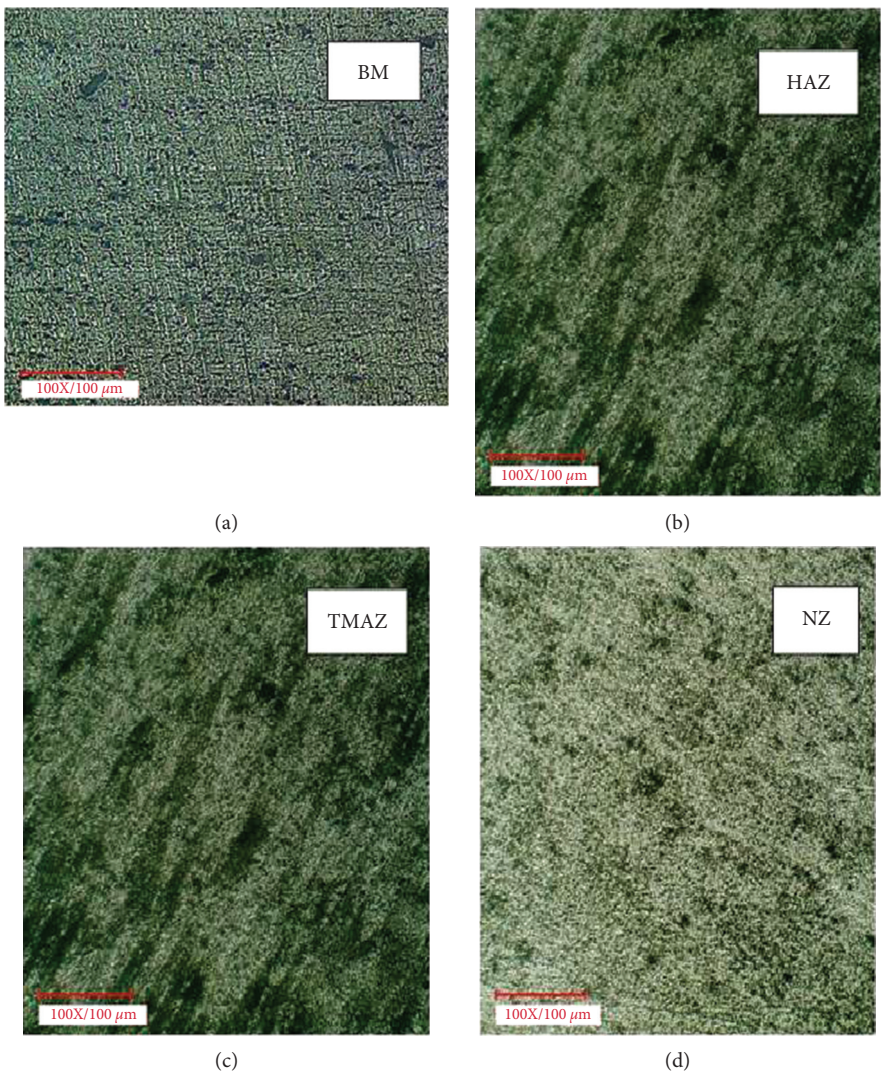

Figure 10: (a) Microstructure of the base metal of AA5052 and (b–d) cross section of the bead-on-plate processed specimen at a tool spinning speed of 1000 rpm, traverse speed of 20 mm/min, and axial load of 5 kN.

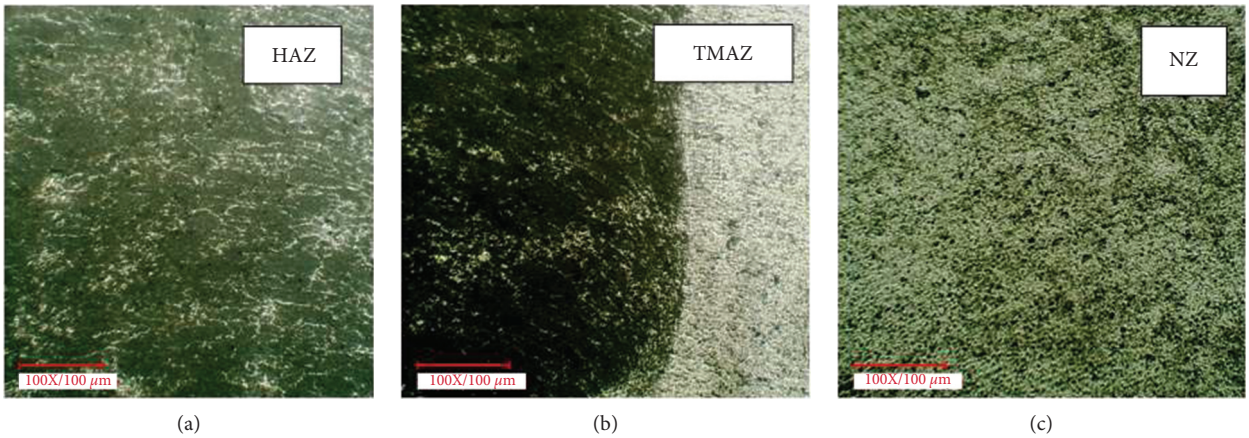

Figure 11: (a–c) Microstructure of cross section of bead-on-plate processed specimen at a tool spinning speed of 1200 rpm, traverse speed of 30 mm/min, and axial load of 5 kN.

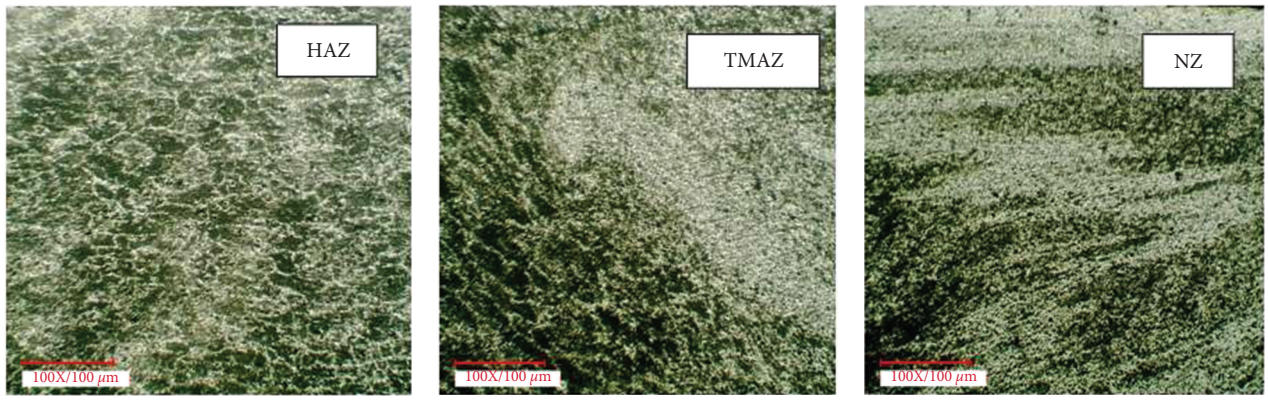

(a) (b) (c)

Figure 12: (a–c) Microstructure of cross section of bead-on-plate processed specimen at a tool spinning speed of 1200 rpm, traverse speed of 20 mm/min, and axial load of 7 kN.

4. Conclusions

This work aimed to examine the effect of friction stir process parameters such as tool spinning speed, traverse speed, and axial load on the tensile strength and microhardness during friction stir bead-on-plate processing. The following conclusions are composed:

(1) The bead-on-plate processing of AA5052 was completed through the friction stir processing technique. The optical micrograph shows the uniform equiaxed grain distributions in the nugget zones of FSPed aluminium alloy 5052.

(2) The S/N ratio of Taguchi technique identifies the optimal process parameters for the friction stir processing of AA5052 to minimize the tensile strength and microhardness, to predict the FSP responses by the developed regression equations.

(3) The optimal process parameters for maximum tensile strength and microhardness were obtained at the tool spinning speed of 1000 rpm, traverse speed of 30 mm/min, and axial load of 5 kN.

(4) The ANOVA outcomes revealed that the tool spinning speed has the most influence as the process parameter on the mechanical properties of the processed specimen, followed by the axial load. The increase in tool spinning speed and axial load leads to an increase in tensile strength.

(5) The microstructure of optimal process parameter limitations displayed the fine grain structure in nugget zones on the surface of the specimen.

(6) The other optimization techniques, such as genetic algorithm and principal component analysis, can be used in the future to optimize the process parameters for enhancing the mechanical properties.

Data Availability

The data used to support the findings of this study are included within the article.

Conflicts of Interest

The authors declare that there are no conflicts of interest regarding the publication of this article.

Acknowledgments

The authors thank the Bharath Institute of Higher Education and Research, Chennai, and this project was supported by researchers supporting project number: RSP-2021/283, King Saud University, Riyadh, Saudi Arabia.

References

[1] P. Cavaliere, G. Campanile, F. Panella, and A. Squillace, "Effect of welding parameters on mechanical and microstructural properties of AA6056 joints produced by friction stir welding," *Journal of Materials Processing Technology*, vol. 180, no. 1–3, pp. 263–270, 2006.

[2] T. Minton and D. J. Mynors, "Utilisation of engineering workshop equipment for friction stir welding," *Journal of Materials Processing Technology*, vol. 177, no. 1–3, pp. 336–339, 2006.

[3] K. Elangovan and V. Balasubramanian, "Influences of tool pin profile and welding speed on the formation of friction stir processing zone in AA2219 aluminium alloy," *Journal of Materials Processing Technology*, vol. 200, no. 1–3, pp. 163–175, 2008.

[4] M. Jayaraman, R. Sivasubramanian, V. Balasubramanian, and A. K. Lakshminarayan, "Optimization of process parameters for friction stir welding of cast aluminium alloy A319 by Taguchi method," *Journal of scientific Industrial Research*, vol. 68, pp. 36–43, 2009.

[5] H. Aydin, B. Ali, U. Esme, Y. Kazancoglu, and O. Guven, "Application of grey relation analysis and Taguchi method for the parametric optimization of friction stir welding process," *Material Technology*, vol. 44, pp. 205–211, 2010.

[6] Z. Lian-Yin, K. Li-Pheng, and Z. Zhao-Wei, "Design concept evaluation in product development using rough sets and grey relation analysis," *Expert Systems with Applications*, vol. 36, no. 3, pp. 7072–7079, 2009.

[7] C. Chi-Hui and L. Wei-Bang, "Thaiping C 2011 Optimal FSW process parameters for aluminum alloys AA5083," *Journal of*

the Chinese Institute of Engineers, vol. 34, no. 1, pp. 99–105, 2011.

[8] S. Mitra, D. Ganguly, B. Acherjee, and A. S. Kuar, "Hole characteristics optimization in Nd:YAG laser micro-drilling of zirconium oxide by grey relation analysis," *International Journal of Advanced Manufacturing Technology*, vol. 610, pp. 1255–1262, 2012.

[9] K. Karun kumar, A. Kumar Kaviti, and N. Kiran Kumar, "Experimental investigation of friction stir welded AA5052 using square and pentagonal tool pins," *Materials Today: Proceedings*, vol. 5, no. 9, pp. 18230–18237, 2018.

[10] S. Shanavas and J. E. R. Dhas, "Quality prediction of friction stir weld joints on AA 5052 H32 aluminium alloy using fuzzy logic technique," *Materials Today: Proceedings*, vol. 5, no. 5, pp. 12124–12132, 2018.

[11] M. Venkateshkannan, V. Rajkumar, P. sadeesh, N. Arivazhagan, S. Narayanan, and K. D. Ramkumar, "Influences of tool geometry on metallurgical and mechanical properties of friction stir welded dissimilar AA 2024 and AA 5052," *Procedia Engineering*, vol. 75, pp. 154–158, 2014.

[12] R. Bharathikanna and G. Elatharasan, "An investigation on microstructures and mechanical properties of AA1050 in friction stir processing technique," *Advance in Natural Applied Science*, vol. 8, pp. 316–321, 2017.

[13] C. Chanakyan and S. Sivasankar, "Parametric advancement of numerical model to predict the mechanical properties of friction stir processed AA5052," *International Journal of Rapid Manufacturing*, vol. 8, no. 1/2, pp. 147–160, 2019.

[14] K. Elangovan, V. Balasubramanian, and M. Valliappan, "Influences of tool pin profile and axial force on the formation of friction stir processing zone in AA6061 aluminium alloy," *International Journal of Advanced Manufacturing Technology*, vol. 38, no. 3-4, pp. 285–295, 2008.

[15] M. Shunmugasundaram, A. Praveen Kumar, L. Ponraj Sankar, and S. Sivasankar, "Optimization of process parameters of friction stir welded dissimilar AA6063 and AA5052 aluminum alloys by Taguchi technique," *Materials Today Proceedings*, vol. 27, 2020.

[16] M. Koilraj, V. Sundareswaran, S. Vijayan, and S. R. Koteswara Rao, "Friction stir welding of dissimilar aluminum alloys AA2219 to AA5083-optimization of process parameters using Taguchi technique," *Materials & Design*, vol. 42, no. 1, 7 pages, 2012.

[17] M. Habibnia, M. Shakeri, S. Nourouzi, and M. K. B. Givi, "Microstructural and mechanical properties of friction stir welded 5050 Al alloy and 304 stainless steel plates," *International Journal of Advanced Manufacturing Technology*, vol. 76, no. 5–8, pp. 819–829, 2015.

[18] G. Ugrasen, G. Bharath, G. K. Kumar, R. Sagar, P. R. Shivu, and R. Keshavamurthy, "Optimization of process parameters for Al6061-Al7075 alloys in friction stir welding using taguchi's technique," *Materials Today: Proceedings*, vol. 5, no. 1, pp. 3027–3035, 2018.

[19] C. Chanakyan, S. Sivasankar, M. Meignanamoorthy, M. Ravichandran, and T. Muralidharan, "Experimental investigation on influence of process parameter on friction stir processing of AA6082 using response surface methodology," *Materials Today: Proceedings*, vol. 21, pp. 231–236, 2020.

[20] C. Chanakyan, P. Dinesh babu, and J. Janarthanan, "An experimental investigation on mechanical properties and microstructure of friction stir welding of AA5052," *Applied Mechanics and Materials*, vol. 48–52, pp. 592–594, 2014.

[21] H. Fujii, L. Cui, M. Maeda, and K. Nogi, "Effect of tool shape on mechanical properties and microstructure of friction stir welded aluminum alloys," *Materials Science and Engineering A*, vol. 419, no. 1-2, pp. 25–31, 2006.

[22] P. L. Threadgill, "Terminology in friction stir welding," *Science and Technology of Welding & Joining*, vol. 12, no. 4, pp. 357–360, 2007.